Pump-Free and Reconfigurable All-Optical Modulation Format Conversion For MQAM Signals by Parallel Nonlinear Mach-Zehnder Interferometers

Qiankun Li, Xiongwei Yang, Huashun Wen, Qi Xu, Yameng Li, Jiali Yang, Huajun Yang, Guangming Zhao, Tianhua Xu, *IEEE Member*

***Abstract*—A pump-free and reconfigurable all-optical modulation format conversion (MFC) scheme for multiple quadrature amplitude modulation (MQAM) signals by the designed parallel nonlinear Mach-Zehnder interferometers (MZIs) is proposed and theory simulated for the first time. In this scheme, the input 30 Gbit/s 8-ary quadrature amplitude modulation (8QAM) signal is divided into two branches by the first 3-dB optical coupler (OC) to get the upper and lower branches 8QAM signals. For the input upper branch 8QAM signal, when it is injected into the designed nonlinear MZI configuration, the first converted quadrature phase shift keying (QPSK1) signal can be obtained. Compared to the input upper branch 8QAM signal, the input lower branch 8QAM signal is firstly sent into an extra piece of highly nonlinear fiber (HNLF) to obtain the pre-perturbed 8QAM signal. When the pre-perturbed 8QAM signal is also injected into the designed nonlinear MZI configuration, the second converted QPSK signal (QPSK2) can be extracted. After adjusting the power ratio (PR) and the relative phase shift (RPS) between QPSK1 and QPSK2, several output optical signals including the aggregated 8QAM (agg-8QAM) signal, the 8-ary phase shift keying (8PSK) signal, the square 8QAM (squ-8QAM) signal, the 8-ary amplitude and phase shift keying (8APSK) signal and the atypical on-off keying (OOK) signal can be obtained from the bar port of the last 3-dB OC. The proposed MFC scheme can also be extended to the other advanced modulation formats including the 40 Gbit/s star 16-ary quadrature amplitude modulation (star-16QAM) signal. The error vector magnitude (EVM) and bit error rate (BER) performance of the input and output optical signals before and after MFC are calculated to analysis the scheme performance. The proposed MFC scheme doesn't need any extra pump which is phase-locked to the input signal. It can also be applied at the intermediate network nodes (INNs) to dynamically select modulation formats suitable for applied between different types of optical networks.**

***Index Terms*—All-optical signal processing, quadrature amplitude modulation, phase shift keying, self-phase modulation, nonlinear Mach-Zehnder interferometer.**

Manuscript received October 26, 2022; revised February 19, 2023 and August 21, 2023; accepted September 15, 2023. (*Corresponding author: Huashun Wen, Huajun Yang and Tianhua Xu.*)

This work was supported in part by National Key R&D Program of China under grants 2019YFB2203104 and 2020YFB2205801 and in part by EU Horizon 2020 MSCA Grant 101008280 (DIOR) and UK Royal Society Grant (IES\R3\223068).

Q. Li and H. Yang are with School of Physics, University of Electronic Science and Technology of China, Chengdu 610054, China. (e-mail: liqk@bupt.cn; yanghj@uestc.edu.cn)

X. Yang is with School of Information and Technology, Fudan University, Shanghai 200433, China. (xwyang22@m.fudan.edu.cn)

H. Wen and G. Zhao are with State Key Laboratory on Integrated Optoelectronics, Institute of Semiconductors, Chinese Academy Sciences, Beijing 100083, China and the School of Electronic, Electrical and Communication Engineering, University of Chinese Academy of Sciences, Beijing 100049, China. (e-mail: whs@semi.ac.cn; gmzhao@semi.ac.cn).

Q. Xu is with School of Information and Electronics, Beijing Institute of Technology, Beijing 100081, China. (e-mail: 3220215105@bit.edu.cn)

Y. Li is with School of Environment, Tsinghua University, Beijing 100084, China. (e-mail: lymxin@126.com)

J. Yang is with School of Information and Communication Engineering, Beijing University of Posts and Telecommunications, Beijing 100876, China. (e-mail: yangjiali@bupt.edu.cn)

T. Xu is with School of Engineering, University of Warwick, Coventry CV4 7AL, United Kingdom, with Tianjin University, Tianjin 300072, China, and also with University College London (UCL), London WC1E 6BT, United Kingdom. (e-mail: tianhua.xu@warwick.ac.uk)

I. INTRODUCTION

WITH the development and application of the fifth-generation (5G) mobile communication technology, Internet of Things (IoT), Internet of Energy (IoE), cloud computing and amounts of data centers (DCs), the low latency flexible optical network (FON) is necessary for the connection between the different DCs and high-speed data transmission [1]–[4]. More and more intelligent terminals with the capacity of edge computing and video upload service motivate the explosive growth of data traffic with different traffic patterns in optical networks. The high-speed data flow are transmitted and processed between long-haul and short-reach optical networks. In order to improve the optical network transmission capacity (NTC), spectrum efficiency (SE) and processing speed, different physics dimensions of lightwaves including amplitude, phase, frequency, polarization and space are utilized to carry the data flow to improve NTC and SE of optical networks. All-optical signal processing (AOSP) technologies including all-optical signal regeneration, wavelength conversion, format conversion, optical encryption/decryption and dynamic bandwidth allocation etc. have been explored in the elastic optical network (EON) to process the data flow in the optical domain to improve the processing speed [5], [6]. While different types of optical networks are allocated to different types of modulation formats according to the network size, NTC and cost [7]. The advanced modulation formats with higher SE and better dispersion tolerance including multiple quadrature amplitude modulation (MQAM) signals and multiple phase shift keying (MPSK) signals have been researched and utilized in different optical networks [8], [9]. However, when the optical signals are transmitted and switched between different types of optical networks, different modulation formats are assigned to the optical signals with spectrum and distance-adaptive at the network gateway. Therefore, all-optical modulation format conversion (MFC) technology has a potential applied advantage at the intermediate network nodes (INNs) in connecting optical networks with different modulation formats [10]–[12].

The MFC function is essential to bridge different types of optical networks at the network gateway [13]. There are three common MFC types: **1.** the advanced modulated signal with higher bit-rate is converted into several simple modulated signals with lower bit-rate [14], [15], **2.** several simple modulated signals are aggregated into one advanced modulated signal [16]–[18], **3.** MFC between different modulated optical signals without changing the modulation depth [19]–[22]. The traditional MFC operation is performed in the electrical domain with the way of optical-electrical-optical (O/E/O) conversion. The signal processing speed will be limited due to the electronic rate bottleneck. In the all-optical network (AON), all the operations are performed in the optical domain by avoiding the O/E/O conversion to achieve a high processing speed. The existing all-optical MFC schemes mainly depend on those nonlinear effects arising from the nonlinear medias with the twice-order and third-order nonlinear susceptibility such as HNLF, semiconductor optical amplifier (SOA), periodically poled lithium niobate (PPLN) and silicon waveguide [14]–[23]. Taking HNLF as an example, the nonlinear effects are mainly considered including self-phase modulation (SPM), cross-phase modulation (XPM) and four-wave mixing (FWM) effects. These nonlinear effects have femtosecond response speed, which can greatly improve the signal processing speed and transmission capacity.

From the perspective of the generation process of nonlinear effects, the XPM and FWM effects need at least one additional pump light to ensure the effective generation of the two nonlinear effects. On one hand, when the extra pump lasers are placed in the transmission links, the system complexity and cost may be increased. On the other hand, the strict phase-matching conditions are usually essential to ensure the effective generation of the FWM effect. These limitations will also increase the MFC scheme complexity. The present MFC schemes mainly concentrate on the first two types based on the XPM and FWM effects, while the extra pump lights are essential. Instead, the SPM effect can be motivated in HNLF independently without the extra pump light when the optical signal is transmitted in the fiber-optic links, which has the potential advantage of simplifying the MFC system complexity. Additionally, there have been many studies reporting the signal regeneration, format conversion and nonlinear phase noise mitigation and other AOSP functions based on the SPM effect without any extra pumps [24]–[26]. For example, the 4-ary amplitude-phase-shift-keying (4APSK) signal and the 8QAM signal have been converted to the binary phase shift keying (BPSK) signal and the quadrature phase shift keying (QPSK) signal separately by designing a nonlinear MZI configuration based on the SPM effect and coherent addition [3], [26].

Recently, 8QAM signals have been recognized the promising modulation formats and proved experimentally in the 100 Gbps optical networks and beyond [27], [28]. Different types of 8QAM signals with different constellation shape have also been investigated [29], [30]. Moreover, different 8QAM modulation formats have been investigated in different optical transmission systems, e. g., adaptive optical OFDM systems, visible light communication (VLC) systems, optical non-orthogonal multiple access (NOMA) systems and passive optical network (PON) systems [31]–[35]. There have also been many schemes talking about the MFC of 8QAM signals, which mainly concentrate on the MFC between the advanced and simple modulated signals [3], [36]–[39]. For instance, the all-optical MFC from one 8QAM to one on-off keying (OOK) and one QPSK have also been investigated by using some nonlinear effects in HNLF and SOA [36]–[38]. In this type of MFC, the intensity information of the inner and the outer rings of the 8QAM are usually transferred into the intensity information of the OOK. The angular phase difference of $\pi/4$ of the 8QAM can be eliminated by the FWM effect in HNLF and the SPM effect and the saturation effect in SOA. Thus, the constellations of the inner and the outer rings of the 8QAM can be converged together to obtain the QPSK signal. While the third MFC type may be more important at the network gateway to bridge the different types of optical networks without changing the modulation depth and inducing the extra pump light. For example, the standard-shaped 8QAM signal with the phase offset of $\pi/4$ between the inner and the outer rings can be deployed in the fiber-optic transmission system and the square-shaped 8QAM signal can be used in the free-space optical transmission system [28], [35]. When the information traffic loaded in the standard-shaped 8QAM signal is transmitted from the fiber-optic transmission system to the free-space optical transmission system, the all-optical format conversion without changing the modulation depth from the standard-shaped 8QAM signal to the square-shaped 8QAM signal need to be performed at the optical gateway. B. Stiller et al. have realized the MFC from star-8QAM (namely 8APSK) signals to 8QAM signals in the high signal-power regime based on phase-sensitive amplification (PSA) with the conjugated pumps [40]. Zhong Z. and Liu H. et al. have reported a format conversion scheme from 8PSK signals to 8QAM signals based on the PSA technology, respectively [39], [41]. Wang H. et al. have improved a format conversion scheme from square 8QAM signals to 8QAM signals with the regeneration function by the coherent mixing of the input optical signal and its high-order conjugated waves [42]. All the above MFC schemes need the extra pumps to ensure the efficient generation of the nonlinear effects. The free of the extra pumps and the phase-matching may have the potential advantage of simplifying MFC configurations.

As far as we know, there are a little schemes simultaneously talking about the MFC from 8QAM signals to 8APSK, 8PSK, square-8QAM and OOK signals. In order to increase the network gateway functions and overcome the above mentioned shortcomings to select the suitable modulation formats to bridge different types of optical networks, a pump-free and reconfigurable all-optical MFC scheme is proposed and simulated for the first time to realize the MFC from 8QAM signals to 8APSK, 8PSK, square-8QAM, and OOK signals by the designed parallel nonlinear MZI configurations based on the SPM effect. The input 30 Gbps 8QAM signal is divided into two branches by the first 3-dB OC. The upper arm 8QAM signal is injected into a SPM-based nonlinear MZI

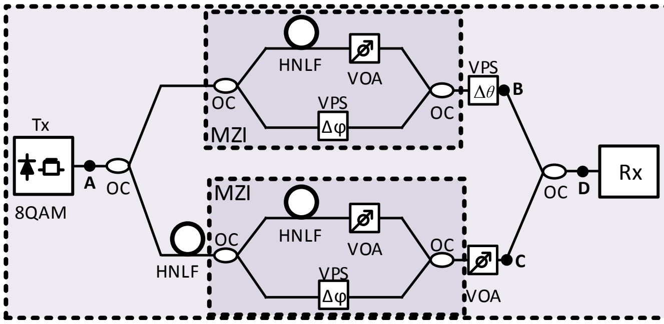

Fig. 1. Function of the proposed simulation scheme, Tx: Transmitter, Rx: Receiver.

configuration to obtain the first converted QPSK signal (QPSK1) by eliminating the inner and the outer rings amplitude difference and phase difference of the input 8QAM signal. The lower arm 8QAM signal is first sent to one piece of HNLF to rotate the inner and the outer rings constellations by the SPM effect to obtain the pre-perturbed 8QAM signal. The pre-perturbed 8QAM signal is also injected into the nonlinear MZI configuration to obtain the second QPSK signal (QPSK2). After adjusting the power ratio (PR) and the relative phase shift (RPS) between the two converted QPSK signals (QPSK1 and QPSK2), they are sent to the last 3-dB OC and coherently superposed to extract the aggregated different types of modulation formats, which include the re-aggregated 8QAM (agg-8QAM), 8APSK, 8PSK, square-8QAM (squ-8QAM) and OOK signals. Moreover, the proposed scheme also has better expansibility to the MFC of MQAM signals with two-ring amplitude states, e. g., star-16QAM signals.

II. Theory and Operating Principles

In order to explain the proposed MFC scheme better, the operation principles are divided into the following section A-B. The whole simulation schematic is shown in Fig. 1.

A. The principle of the nonlinear MZI configuration

The nonlinear MZI configuration has been explored in the MFC [43], all-optical pulse switching [44], regeneration [45] and so on. The designed nonlinear MZI simulation configuration is composed by two 3-dB OCs, one HNLF and one directional variable optical attenuator (VOA) in the upper branch, one directional variable phase shifter (VPS) in the lower branch. In the practical experiment, one tunable optical delay line (TODL) in the lower branch with the same length as the HNLF in the upper branch usually can be used to ensure that the upper and lower branches optical pulses are bit-aligned when coherently superposed. When the input optical signal transmits in the nonlinear MZI configuration, the input optical signal is divided into two components through the first 3-dB OC to get the upper and lower branches optical signals. The two components of the input optical signal experience the different linear and nonlinear phase shifts induced by the SPM effect [46]. The constellations of the input optical signal with a higher intensity obtains a big SPM phase shift and which with a lower intensity gets a small SPM phase shift. The VPS in the lower branch can not only be used to compensate for the phase shift difference brought by the HNLF used in the upper branch, but also adjust the relative phase states of the upper and lower branch optical signals when coherently superposed. The VOA in the upper branch is used to adjust the optical signal power with a SPM phase shift. Thus, the two adjusted components are superposed coherently in the second 3-dB OC of the nonlinear MZI configuration. When the optical signal is coherently superposed with itself, the high amplitude is attenuated due to the big SPM phase shift. Similarly, the small amplitude is also attenuated due to the small SPM phase shift. The high and the small amplitudes can be converged into the same amplitude level. The phase distribution of the converged optical signal is dependent on the angle of the coherent addition between the upper and lower branches components. After adjusting the VPS, the constellations with the high and the small intensities of the input 8QAM signal with the different phase states can also be converged into the same phase level.

Noteworthily, this paper reveals the format conversion from the input 8QAM signal to two converted QPSK signals in theory. In the real experiment of the nonlinear MZI configuration, it is distorted easily by the phase drift between the upper and lower arms brought by the temperature, airflow, vibration, curvature and splitting ratio of OC. Some active and passive phase-stability operations and configurations are necessary for the nonlinear MZI configuration, for instance, the active feedback stabilization by the piezoelectric (PZT) fiber stretcher and the passive nonlinear optical loop mirror (NOLM), et al. [47]–[49].

The mathematical relationship between the input and output ports of the 3-dB OC can be written as:

$$\begin{pmatrix} E_{1,out} \\ E_{2,out} \end{pmatrix} = \frac{\sqrt{2}}{2} \begin{pmatrix} 1 & i \\ i & 1 \end{pmatrix} \cdot \begin{pmatrix} E_{1,in} \\ E_{2,in} \end{pmatrix} \tag{1}$$

$E_{1,in}$, $E_{2,in}$ represent the electric fields of the input optical signals, respectively. $E_{1,out}$, $E_{2,out}$ represent the electric fields of the output optical signals, respectively. In the designed nonlinear MZI simulation configuration, there is only one input 8QAM signal, which can be represented by $E_{1,out}$. While $E_{2,out}$ is null. For the first 3-dB OC, the output upper branch signal can be expressed as:

$$E_{1,out} = \frac{\sqrt{2}}{2} E_{1,in} \tag{2}$$

The output lower branch signal can be written as:

$$E_{2,out} = i \frac{\sqrt{2}}{2} E_{1,in} \tag{3}$$

The electrical field of the input 8QAM signal can be written as:

$$E_{1,in} = A_{in} \cdot e^{i\varphi_{in}} \tag{4}$$

A_{in} and φ_{in} represent the amplitude and the phase of the 8QAM signal. When the input 8QAM signal is transmitted in HNLF, the SPM phase shift induced by its inner and outer rings can be expressed as:

$$\varphi_{spm}^{k} = \gamma L_{eff} P_k \tag{5}$$

Where γ and L_{eff} represent the nonlinear coefficient and effective length of the used HNLF separately. P_k represents the inner and the outer rings power of the 8QAM signal, respectively. Due to the nonlinear index of TODL is far less than that of HNLF, the nonlinear phase shift brought by TODL is ignored whether in the theory derivation and numerical simulation.

When the output upper branch 8QAM signal from the first 3-dB OC is transmitted to the HNLF and VOA without consideration of the fiber loss, the electrical field of the output optical signal can be written as:

$$E'_{1,out} = E_{1,out} \cdot e^{i\varphi_{spm}} \cdot 10^{-\frac{\alpha}{20}} \tag{6}$$

φ_{spm} represents the SPM phase shift, and its expression is the similar as Equation (5). α represents the attenuation coefficient of the directional VOA. When the output lower branch 8QAM signal from the first 3-dB OC is transmitted to the VPS, the electrical field of the output optical signal can be expressed as:

$$E'_{2,out} = E_{2,out} \cdot e^{-i\Delta\varphi} \tag{7}$$

$\Delta\varphi$ represents the phase shift of the directional VPS. After the output upper and lower optical signals are coherently added again in the second 3-dB OC of the designed nonlinear MZI configuration, the output optical filed from the bar port of the second 3-dB OC can be written as:

$$\begin{aligned} E_{out} &= \frac{\sqrt{2}}{2}E'_{1,out} + i\frac{\sqrt{2}}{2}E'_{2,out} \\ &= \frac{1}{2}A_{in}[e^{i(\varphi_{in}+\varphi_{spm})} \cdot 10^{-\frac{\alpha}{20}} - e^{i(\varphi_{in}-\Delta\varphi)}] \end{aligned} \tag{8}$$

The output optical signal power of the nonlinear MZI configuration, namely, the power transfer function (PTF) between the output and input optical signals can be written as:

$$P_{out} = \frac{1}{4}P_{in}[1 + 10^{-\frac{\alpha}{10}} - 2 \cdot 10^{-\frac{\alpha}{20}} cos(\varphi_{spm} + \Delta\varphi)] \tag{9}$$

P_{in} represents the input signal power. For the input 8QAM signal, P_{in} can be the inner and the outer rings power of the 8QAM signal, respectively. In order to reveal the phase variation characteristic of the output optical signal, the transmission coefficient (TC) is defined as the ratio of the output optical signal to the input optical signal:

$$TC = \frac{E_{out}}{E_{in}} = \frac{1}{2} \cdot e^{i\varphi_{spm}} \cdot 10^{-\frac{\alpha}{20}} - \frac{1}{2} \cdot e^{-i\Delta\varphi} \tag{10}$$

The phase of TC represents the RPS between the output and the input optical signals, which can be expressed as:

$$\Delta\varphi_t = arctan\frac{10^{-\frac{\alpha}{20}} \cdot sin\varphi_{spm} + sin\Delta\varphi}{10^{-\frac{\alpha}{20}} \cdot cos\varphi_{spm} - cos\Delta\varphi} \tag{11}$$

Obviously, the RPS of the nonlinear MZI configuration is independent with the phase of the input optical signal, but dependent with the input optical signal power. The amplitude noise of the input optical signal would be transferred to the optical phase noise of the output optical signal.

The PTF of the output optical signal from the designed nonlinear MZI is dependent on the power of the input 8QAM signal, the nonlinear index and effective length of the HNLF used, VOA and VPS in the upper and lower arms.

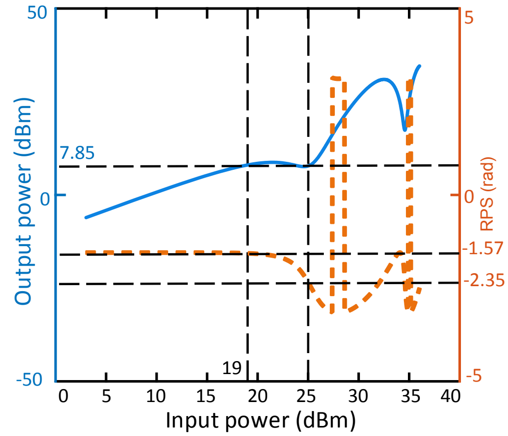

Fig. 2. (a) PTF and (b) RPS of the designed nonlinear MZI configuration.

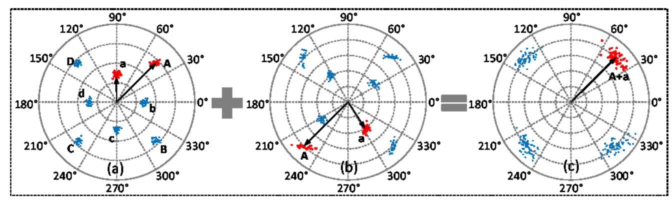

Fig. 3. Constellations of (a) the input 8QAM signal, (b) the input 8QAM signal with SPM phase shift and (c) the first converged QPSK signal (QPSK1) in the designed nonlinear MZI configuration.

The PTF and RPS curves of the nonlinear MZI configuration have been plotted in Fig. 2. When the input optical signal average power is 23 dBm, the corresponding power for the inner and the outer rings constellations of the input 8QAM signal are 19 dBm and 25 dBm. From the curve of PTF, the corresponding output power for input the inner and the outer ring power of 19 dBm and 25 dBm are both 7.85 dBm. The power of the inner and the outer rings constellations of the input 8QAM signal can be converged to the same output power. This means the constellations of the input 8QAM signal with two-levels amplitude can be converted to the constellations with one-level amplitude. When the input power is 19 dBm, the corresponding RPS is about -1.57 rad. When the output power is about 25 dBm, the corresponding RPS is -2.35 rad. The extra phase shift difference is about 0.78 rad. Since the adjacent angular distance between the inner and the outer rings constellations of the input 8QAM signal is $\pi/4$, which can be compensated by the extra phase shift difference. This means the phase difference between the inner and the outer rings constellations of the input 8QAM signal can be eliminated by the nonlinear MZI configuration. Since the inner and the outer rings constellations of the input 8QAM signal have been converged together by the nonlinear MZI configuration, the phase difference between the inner and the outer rings constellations of the input 8QAM signal is erased to obtain the output optical signal from the nonlinear MZI. To sum up, the input 8QAM signal with two rings and the adjacent angular distance of $\pi/4$ can be converted into the

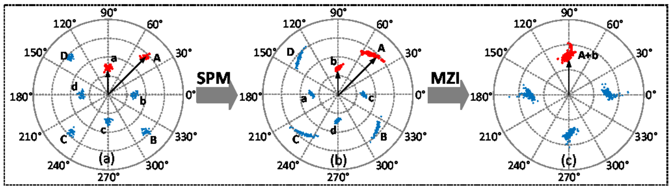

Fig. 4. Constellations of the (a) input 8QAM signal, (b) the pre-perturbed 8QAM signal by the SPM effect and (c) the second converged QPSK signal (QPSK2).

output QPSK signal with one ring.

In order to further observe the converge function of the designed nonlinear MZI configuration, the input 8QAM signal is taken as an example to verify. The constellations of the input 8QAM signal, the upper branch 8QAM signal with SPM phase shift and the converted QPSK signal are plotted in Fig. 3. The constellations in the inner ring are represented by a, b, c, d, while the constellations in the outer ring are represented by A, B, C, D. When the signal constellations in Fig. 3 (a) are coherently added with the signal constellations in Fig. 3 (b), the constellation points A and a are converged together in Fig. 3 (c), that is A+a. Compared with the constellation points A and a before convergence, the converged constellation points (A+a) have only one amplitude state and one phase state. This processing can be viewed as the MFC from the input 8QAM signal to the output first QPSK signal (QPSK1).

In order to ensure the information integrity of the input 8QAM signal, another nonlinear MZI configuration is used to convert the input 8QAM signal into the second QPSK signal (QPSK2). A piece of HNLF is set before the nonlinear MZI configuration to pre-perturb the input 8QAM signal to obtain the pre-perturbed 8QAM signal with about $\pi/2$-SPM phase shift between the inner and the outer rings constellations. The constellations before and after pre-perturbed by SPM phase shift are plotted in Fig. 4 (a)-(b). The outer ring constellations have the high intensity, which lead to a big SPM phase shift. While the inner ring constellations have the low intensity, which induce a small SPM phase shift. When the SPM phase shift difference between the inner and the outer rings constellations is about $\pi/2$, the pre-perturbed 8QAM signal maintains the same constellations distribution in amplitude states and phase states as the input 8QAM signal. Thus, when the pre-perturbed 8QAM signal is transmitted through the nonlinear MZI configuration, the constellation points A and constellation points b are converged into the new constellation points A+b, as shown in Fig. 4 (c). Obviously, the amplitude difference and phase difference of the inner ring constellation points b and the outer constellation points A are eliminated. The two amplitude levels of A and b are converged into one amplitude level. The two phase states of A and b are converged into one phase state. This processing can be viewed as another MFC from the 8QAM signal to the second QPSK signal (QPSK2). The two QPSK signals include all the information induced in the input 8QAM signal.

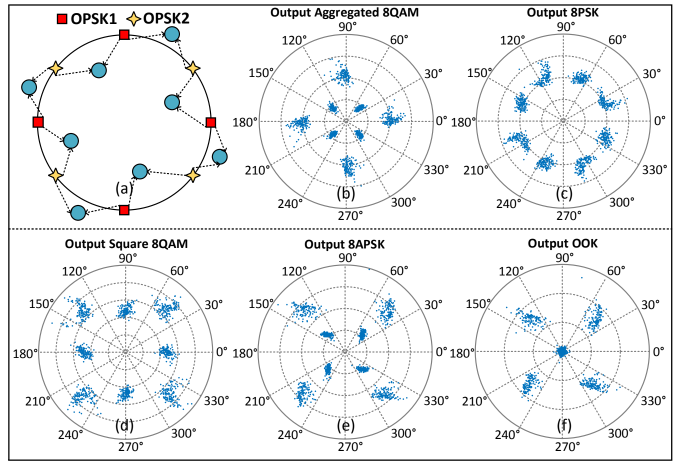

Fig. 5. (a) Constellation diagrams of coherent addition between QPSK1 and QPSK2, (b) output aggregated 8QAM signal, (c) output 8PSK signal, (d) output square 8QAM signal, (e) output 8APSK signal and (f) output atypical OOK signal.

B. The principle of coherent addition between the two converged QPSK signals

The second 3-dB OC is used to realize the coherent superposition between the two converged QPSK signals. Since the upper and lower arms nonlinear MZI configurations have the same parameters, the time delay between the converted QPSK1 and QPSK2 is mainly brought by the HNLF used for pre-perturbing the input 8QAM signal. Therefore, in the real experiment, one TODL with the same length as the pre-perturbed HNLF may be set after the upper arm nonlinear MZI to compensate for the time delay. From Fig. 3 (c) and Fig. 4 (c), the converged constellation points A+a of QPSK1 and the constellation points A+b of QPSK2 both have the information induced in the constellation points A. Although both QPSK1 and QPSK2 represent two bits of information per symbol, they don't represent four bits of information after coherent superposition. The coherent addition process is shown in Fig. 5 (a). A VPS is set after QPSK1 and a VOA is set after QPSK2 to adjust the power and relative phase difference of QPSK1 and QPSK2. Various kinds of the output aggregated optical signals can be obtained through coherent addition from the bar port of the 3-dB OC. The electrical field of the output optical signal can be expressed as:

$$E_{out}^{bar} = \frac{\sqrt{2}}{2}(A_{qpsk1} \cdot e^{i\varphi_{qpsk1}} + iA_{qpsk2} \cdot e^{i\varphi_{qpsk2}}) \quad (12)$$

A_{qpsk1} and A_{qpsk2} represent the amplitudes of QPSK1 and QPSK2. φ_{qpsk1} and φ_{qpsk2} represent the phases of QPSK1 and QPSK2. The output optical signal power can be written as:

$$P_{out} = \frac{1}{2}P_1 + \frac{1}{2}P_2 + \sqrt{P_1P_2}sin(\varphi_{qpsk1} - \varphi_{qpsk2}) \quad (13)$$

P_1 and P_2 represent the average power of QPSK1 and QPSK2. When the electrical field phase of the converged QPSK1 and QPSK2 satisfy the constant relation of φ_{qpsk1}=φ_{qpsk2}+$\Delta\psi$, the output optical power can be modified as:

$$P_{out} = \frac{1}{2}P_1 + \frac{1}{2}P_2 + \sqrt{P_1 P_2} sin(\Delta\psi) \tag{14}$$

$\Delta\psi$ represents the relative phase difference between φ_{qpsk1} and φ_{qpsk2}. The output optical phase can be written as:

$$\varphi_{out} = arctan\frac{A}{B} \tag{15}$$

where:

$$\begin{cases} A = \sqrt{P_1} tan\varphi_{qpsk2} cos\Delta\psi + \sqrt{P_1} sin\Delta\psi + \sqrt{P_2} \\ B = \sqrt{P_1} cos\Delta\psi - \sqrt{P_1} tan\varphi_{qpsk2} sin\Delta\psi \\ -\sqrt{P_2} tan\varphi_{qpsk2} \end{cases} \tag{16}$$

When φ_{qpsk2}=[$\frac{\pi}{4}$,$\frac{3\pi}{4}$,$\frac{5\pi}{4}$,$\frac{7\pi}{4}$], the output optical phase can be modified as:

$$\varphi_{out} = arctan\frac{C}{D} \tag{17}$$

where:

$$\begin{cases} C = \sqrt{P_1} \cdot sign(\varphi_{qpsk2}) cos\Delta\psi + \sqrt{P_1} sin\Delta\psi + \sqrt{P_2} \\ D = \sqrt{P_1} cos\Delta\psi - \sqrt{P_1} \cdot sign(\varphi_{qpsk2}) sin\Delta\psi \\ -\sqrt{P_2} \cdot sign(\varphi_{qpsk2}) \end{cases} \tag{18}$$

When the $sign(\varphi_{qpsk2})$=1, the Equation (15) can be written as:

$$\varphi_{out} = arctan\frac{\sqrt{P_1} cos\Delta\psi + \sqrt{P_1} sin\Delta\psi + \sqrt{P_2}}{\sqrt{P_1} cos\Delta\psi - \sqrt{P_1} sin\Delta\psi - \sqrt{P_2}} \tag{19}$$

When the $sign(\varphi_{qpsk2})$=-1, the Equation (15) can be written as:

$$\varphi_{out} = arctan\frac{-\sqrt{P_1} cos\Delta\psi + \sqrt{P_1} sin\Delta\psi + \sqrt{P_2}}{\sqrt{P_1} cos\Delta\psi + \sqrt{P_1} sin\Delta\psi + \sqrt{P_2}} \tag{20}$$

The input 8QAM signal can be re-aggregated through the coherent addition of the two converged QPSK signals when the VPS and VOA are set to be 0, as shown in Fig. 5 (b). The output 8PSK signal can be obtained when the VPS is changed into π/2 and the VOA is set to be 0, as shown in Fig. 5 (c). The output square 8QAM signal can be extracted when the VPS is made into π/4 and the VOA is set to be 0, as shown in Fig. 5 (d). The output 8APSK signal can be received when the VPS is changed into -π/9 and the VOA is set to be 5 dB, as shown in Fig. 5 (e). The output atypical OOK signal can be got when the VPS is set to be -π/4 and the VOA is maintained to be 0, as shown in Fig. 5 (f). The atypical OOK signal can be viewed as the gated QPSK signal, which has the advantage of reducing the available time slot [50].

III. Simulation and discussion

The proposed MFC scheme of the input 30 Gbit/s 8QAM signal is shown in Fig. 1. The input 8QAM signal at the frequency of 193.1 THz is generated by phase modulators (PM) (modulated index: π, π/2 and π/4) and amplitude modulators (AM) (modulated index: 0.75) driven by pseudo-random binary sequence (PRBS). The non-return-to-zero (NRZ) coder generates a sampled NRZ coded signal defined by a train of bit sequence generated by the PRBS module at its input. A Gaussian filter transforms rectangular electrical input pulses into smoother output pulses with a rise time of 2.5×10^{-11} s. Notably, the input 8QAM signal can also be generated by using I/Q modulator. The optical-signal-noise-ratio (OSNR) of the input 8QAM signal is changed by an amplifier spontaneous emission (ASE) noise source. A 3-dB OC is used to divide the input 8QAM signal into the upper and lower branches. The upper branch 8QAM signal with the input average power of 23 dBm is sent into the designed nonlinear MZI configuration to extract the first QPSK signal (QPSK1). The HNLF used in the nonlinear MZI upper branch is 375 m with a nonlinear coefficient of 13.1 $(\mathrm{W\cdot km})^{-1}$, the attenuation coefficient of 0.2 dB/km, the dispersion coefficient of 16×10^{-6} ps/(nm·km) and the dispersion slope of 0.02 ps/((nm)^2·km)). For the inner and the outer rings constellations of the input 8QAM signal, the corresponding nonlinear phase shifts are about 0.39 rad and 1.55 rad, respectively. The VOA and VPS in the upper and lower branches of the nonlinear MZI are set to 2.8 dB and -π/4, respectively. QPSK1 can be filtered out by the optical band pass filter (OBPF, f_c=193.1 THz) from the nonlinear MZI. While the lower branch 8QAM signal with the input average power of 23 dBm is firstly injected into one piece of HNLF to obtain the pre-perturbed 8QAM signal. The HNLF used (the reference frequency: 193.1 THz, the nonlinear coefficient of 13.1 $(\mathrm{W\cdot km})^{-1}$, the attenuation coefficient of 0.2 dB/km, the dispersion coefficient of 16×10^{-6} ps/(nm·km) and the dispersion slope of 0.02 ps/((nm)^2·km)) has a length of 480 m. Therefore, the corresponding nonlinear phase shifts of the inner and the outer rings of the 8QAM signal generated by the pre-perturbed HNLF are about 0.5 rad and 1.99 rad, respectively. The second QPSK signal (QPSK2) can be extracted by another OBPF (f_c=193.1 THz) when the pre-perturbed 8QAM signal is also sent into the designed nonlinear MZI configuration. The constellations of the input 8QAM signal, two converted QPSK signals are plotted and shown in Fig. 6 with an input OSNR of 25 dB. Moreover, the wavelengths of the two converted QPSK signals (QPSK1 and QPSK2) are the same with the input 8QAM signal. This can avoid to use the wavelength conversion configuration and improve the single carrier utilization.

The encoding rules for 8QAM signals are generally different depending on their generation methods and modulation format types. In the proposed scheme, the phase mapping and logic relations between the input 8QAM signal and the two converted QPSK signals are summarized in TABLE I. It is obvious that there seems more information in two QPSK signals (2×2 bits per symbol) than in the input 8QAM signal (3 bits per symbol), i. e., the process introduces some redundancy. However, the two QPSK signals have some correlation in phase mapping and logic relations. By observing the binary data encoded on the input 8QAM signal and that on the two converted QPSK signals, we can find the first two bits of the input 8QAM signal have an identical logic relation with QPSK2, and the last bit of the input 8QAM signal is only same with the last bit of QPSK1. Therefore, the first binary data on QPSK1 is a redundant bit. However, the redundancy does not affect the dependence of the original information carried by the converted QPSK signals. It only brings special decoding rules for QPSK1, i. e., the phase states '-π/4' and '3π/4' of

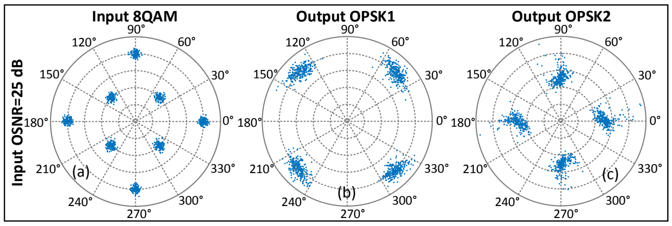

Fig. 6. Constellation diagrams of (a) the input 8QAM signal, (b) the converted QPSK1 signal, (c) the converted QPSK2 signal.

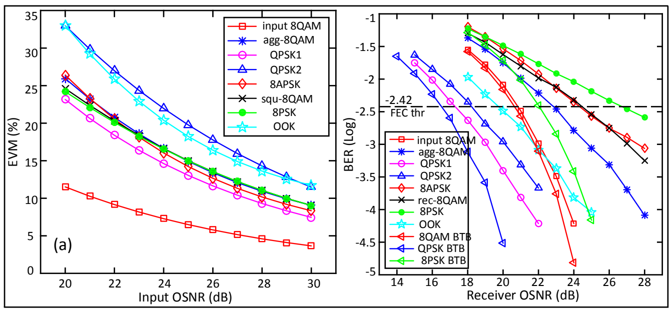

Fig. 7. (a) EVM vs input OSNR; (b) BER vs receiver OSNR; agg-8QAM: aggregated 8QAM; squ-8QAM: square 8QAM.

QPSK1 represent the binary data '0', and the phase states '$\pi/4$' and '-$3\pi/4$' represent the binary data '1'. In this way, the last bit of the input 8QAM signal can still be identified correctly. More importantly, the simultaneous format conversion from the input 8QAM signal to two QPSK signals can be realized and no loss of the information happens in the process.

A VPS is set after QPSK1 to compensate for the extra phase shift induced by the HNLF used which is used to generate the pre-perturbed 8QAM signal and adjust the angle of coherent addition between QPSK1 and QPSK2. A VOA is set after QPSK2 to adjust the power ratio of coherent addition between QPSK1 and QPSK2. Thus the several aggregated output optical signals can be obtained through the bar port of the last 3-dB OC. The constellations of the several aggregated optical signals have been shown in Fig. 5 (b)-(f) with an input OSNR of 25 dB.

The scheme EVM performance is evaluated by measuring 2^{10} signal symbols with the input OSNR of 8QAM signal changes from 20 dB to 30 dB. As shown in Fig. 7 (a), with the increase of the input OSNR, the EVM performance of the input 8QAM signal is better than the two converted QPSK signals and other several aggregated optical signals including atypical OOK signals, 8APSK signals, 8PSK signals and square 8QAM signals etc. QPSK1 has better EVM performance than QPSK2 due to the lacking of pre-perturbation by SPM phase shift. QPSK2 accumulates a lot of nonlinear amplitude and phase noise compared to QPSK1 thanks to the pre-perturbation processing. With the input OSNR of 25 dB, the EVM performance of the input 8QAM signal, QPSK1, QPSK2, the aggregated 8QAM signal, the 8PSK signal, the square 8QAM signal, the 8APSK signal and the atypical OOK signal are 6.49%, 13.05%, 19.77%, 14.91%, 14.98%, 15%, 14.23% and 18.23%. respectively.

The ASE noise source is added at the point A, B, C and D with the input 8QAM signal, two converted QPSK signals and output aggregaed optical signals to change the receiver OSNR before signal detection. Thus the scheme BER performance is calculated by measuring 2^{17} signal symbols when the receiver OSNR varies from 15 dB to 28 dB with the input OSNR of 25 dB. When the hard decision forward-error-correction threshold (HD-FEC thr) is set to be $\log_{10}{}^{(3.8\times10^{-3})} = -2.42$, the receiver OSNR of the input 8QAM signal, QPSK1, QPSK2, the aggregated 8QAM signal, the 8PSK signal, the square 8QAM signal, the 8APSK signal and the atypical OOK signal are about 20.8 dB, 17.3 dB, 18.2 dB, 22.8 dB, 26.8 dB, 24.4 dB, 24.3 dB and 19.8 dB, respectively. Notably, whether the input and output optical signals before and after format conversion can be decodable if the HD-FEC threshold of $\log_{10}{}^{(3.8\times10^{-3})} = -2.42$ is used, it does not prevent us from using $\log_{10}{}^{(3.8\times10^{-3})} = -2.42$ as a measure to compare the performance of modulation format conversion schemes. This is because the BER performance of the input and output optical signals before and after format conversion are measured directly by comparing the bit sequences of the transmitter and the receiver. As shown in Fig. 7 (b), QPSK1 and QPSk2 have 3.5 dB and 2.6 dB improvement, respectively, in the receiver OSNR compared to the input 8QAM signal. At the HD-FEC of -2.42, the theoretical required OSNR of the ideal input 8QAM, 8PSK and QPSK signals with back-to-back (BTB) transmission are about 20.6 dB, 22 dB and 16.5 dB by calculating 2^{17} signal symbols, respectively. Compared to the ideal 8QAM signal with BTB transmission, the input 8QAM signal with an OSNR of 25 dB has about 0.2 dB penalty in the receiver OSNR. Compared to the ideal 8PSK signal with BTB transmission, the converted 8PSK signal from the input 8QAM signal with an OSNR of 25 dB has about 4.8 dB penalty in the receiver OSNR. Compared to the ideal QPSK signal with BTB transmission, the converted QPSK1 and QPSK2 have about 0.8 dB and 1.7 dB penalty in the receiver OSNR, respectively. Although the EVM performance of QPSK1 and QPSK2 decreased compared to the input 8QAM signal, BER performance improved. On one hand, the bit rate of QPSK1 and QPSK2 is reduced compared to the input 8QAM signal, on the other hand, the QPSK signal has better anti-noise ability as a low order modulated signal. The Euclidean distance between the adjacent constellations of the QPSK signal is larger than that of the 8QAM signal. The 0.9 dB receiver OSNR gap between QPSK1 and QPSK2 is caused by the extra SPM phase shift induced by the pre-perturbed HNLF.

Compared to the 8QAM signal with an input OSNR of 25 dB, the aggregated OOK signal has the receiver OSNR improvement of 1 dB. The aggregated OOK signal as a gated QPSK signal has better BER performance than the input 8QAM signal when the receiver OSNR is less than about 22 dB. This proves the aggregated OOK signal is more suitable to transmit in the long-haul fiber-optic links, which is formed by multi-span fiber and multiple erbium doped fiber application amplifiers (EDFAs) with ASE noise. The input 8QAM signal is more suitable than the aggregated OOK signal in the medium and short distance optical transport network.

TABLE I
THE OPTICAL PHASE MAPPING AND LOGIC PATTERN BETWEEN THE INPUT 8QAM SIGNAL AND THE TWO CONVERTED QPSK SIGNALS

8QAM			QPSK1			QPSK2		
logic	phase	amplitude	logic	phase	amplitude	logic	phase	amplitude
111	$\pi/4$	A1	11	$\pi/4$	A3	11	0	A4
101	$\pi/2$	A2	11	$\pi/4$	A3	10	$\pi/2$	A4
011	$-\pi/2$	A2	01	$-3\pi/4$	A3	01	$-\pi/2$	A4
001	$-3\pi/4$	A1	01	$-3\pi/4$	A3	00	π	A4
110	0	A2	10	$-\pi/4$	A3	11	0	A4
100	$3\pi/4$	A1	00	$3\pi/4$	A3	10	$\pi/2$	A4
010	$-\pi/4$	A1	10	$-\pi/4$	A3	01	$-\pi/2$	A4
000	π	A2	00	$3\pi/4$	A3	00	π	A4

TABLE II
THE VARIANCE IN RECEIVER OSNR FOR THE CONVERTED OPTICAL SIGNALS COMPARED TO THE 8QAM SIGNAL WITH AN INPUT OSNR OF 25 DB

Converted Signal	Variance in Receiver OSNR
QPSK1	Improvement of 3.5 dB
QPSK2	Improvement of 2.6 dB
Aggregated 8QAM	Penalty of 2 dB
Aggregated 8APSK	Penalty of 3.5 dB
Aggregated Square 8QAM	Penalty of 3.6 dB
Aggregated OOK	Improvement of 1 dB
Aggregated 8PSK	Penalty of 6 dB

The BER performance of the aggregated 8QAM signal, the 8SPK signal, the square 8QAM signal and the 8APSK signal are worse than the input 8QAM signal with the increase of the receiver OSNR. The square 8QAM signal and the 8APSK signal have the similar BER performance.

For the aggregated 8QAM signal and the 8PSK signal, there are 2 dB and 6 dB penalty in the receiver OSNR compared to the input 8QAM signal. As such, compared to the aggregated 8QAM signal, the aggregated 8PSK signal has about 4 dB penalty in the receiver OSNR. For the aggregated square 8QAM signal and the 8APSK signal, there is about 3.6 dB and 3.5 dB penalty, respectively, in the receiver OSNR compared to the input 8QAM signal. The accumulated nonlinear amplitude and phase noise brought by the SPM phase shift and coherent addition degrade the quality of the aggregated optical signals. This MFC from the input 8QAM signal to the several aggregated optical signals can also be viewed as the geometric constellation shaping (GCS) for the input 8QAM signal. Although the probability constellation shaping (PCS) is being the common option for many networks, the GCS is also beneficial to the dynamic and reconfigurable optical transport network, which can select the suitable modulation format according to the network size, receiving device and cost etc. In order to observe the variance of the receiver OSNR of the input 8QAM signal and the format converted signals, the improvement and the penalty in the receiver OSNR of the input and the output signals are listed, as shown in TABLE II.

The proposed scheme can also be extended to the MFC for the input 40 Gbit/s star-16QAM and more advanced star-MQAM signals with two rings. Taking the input star-16QAM signal as an example, the constellation diagrams of the input star-16QAM signal, two converted 8PSK signals, aggregated star-16QAM signal and atypical OOK signal (namely gated 8PSK signal) with the input OSNR of 30 dB are plotted in Fig. 8. The two converted 8PSK signals as the simple modulated signals with a constant envelope have better tolerance for the nonlinear phase shift than the input star-16QAM signal. Moreover, when the differential coding rules are made, the two converted differential 8PSK signals may be received by direct detection (DD). For the aggregated star-16QAM signal and the output atypical OOK signal, the former keeps the information integrity and the latter has a higher extinction than the input star-16QAM signal between the inner and the outer rings.

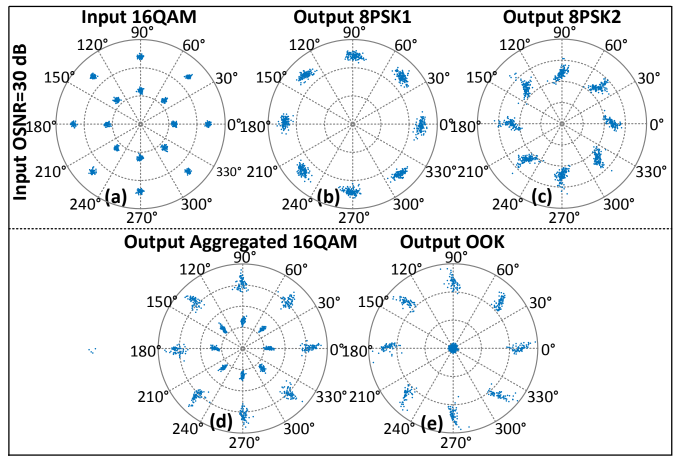

Fig. 8. Constellation diagrams of (a) the input star-16QAM signal, (b) the converted 8PSK1 signal, (c) the converted 8PSK2 signal, (d) the aggregated star-16QAM signal and (e) the output atypical OOK signal.

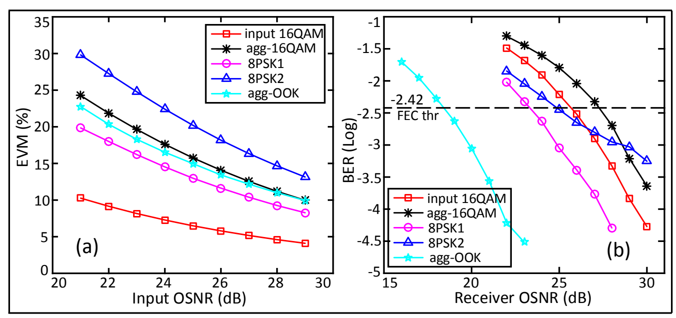

Fig. 9. (a) EVM vs input OSNR; (b) BER vs receiver OSNR; agg-16QAM: aggregated 16QAM; agg-OOK: aggregated atypical OOK.

2^{14} signal symbols are counted to measure the EVM performance for the input star-16QAM signal before and after de-aggregation and aggregation to evaluate the scheme performance, respectively, as shown in Fig. 9 (a). When the input OSNR sweeps from 21 dB to 29 dB, the two converted

8PSK signals and aggregated atypical OOK signal have worse EVM performance than the input star-16QAM signal. This is mainly caused by the amplitude noise and nonlinear phase noise brought by the SPM effect. Especially, the pre-perturbed 8QAM signal also obtains the extra noise distortion, which directly lead to the EVM performance of 8PSK2 is worse than 8PSK1. When the input OSNR lies in 29 dB, the EVM performance of the input star-16QAM signal, 8PSK1, 8PSK2 and output aggregated star-16QAM signal and atypical OOK signal are 6.49%, 12.99%, 20.21%, 15.76% and 14.98%, respectively.

2^{17} signal symbols are measured to calculate the system BER performance when the receiver OSNR varies from 16 dB to 30 dB with the input OSNR of 30 dB, as shown in Fig. 9 (b). Under the condition of HD-FEC, the receiver OSNR of the input star-16QAM signal, 8PSK1, 8PSK2, aggregated star-16QAM signal and aggregated atypical OOK signal are about 25.6 dB, 23.4 dB, 25 dB, 27.3 dB and 18.5 dB, respectively. Compared to the ideal 8PSK signal with BTB transmission, the two converted 8PSK signals have about 1.4 dB and 3 dB penalty in the receiver OSNR, respectively. Although the converted two 8PSK signals and aggregated OOK signal have worse EVM performance, the converted two 8PSK signals and aggregated atypical OOK signal have better BER performance than the input star-16QAM signal. 8PSK and OOK signals as the low-order modulated formats have bigger Euclidean distance between the adjacent constellations than the input star-16QAM signal. The receiver OSNR gap of 1.6 dB between 8PSK1 and 8PSK2 is also mainly caused by the by the extra SPM phase shift induced by the pre-perturbed HNLF. The aggregated OOK signal can obtain about 7.1 dB receiver OSNR performance improvement compared to the input star-16QAM signal. While for the aggregated star-16QAM signal, there is about 1.7 dB receiver OSNR penalty compared to the input star-16QAM signal. This penalty mainly results from the accumulated amplitude and phase noise brought by the SPM effect and coherent addition.

In the practical experiment, the phase drift, time delay, variation between the two different arms and other environment factors must be considered. Some active and passive methods have been mentioned for stabling the phase drift of the nonlinear MZI in the Section A. When the two converted QPSK signals are coherently superposed, the time delay brought by the lower arm pre-perturbed HNLF is also needed to be compensated. One of the solutions is that one TODL is set after the first converted QPSK signal to ensure the synchronous between the converted QPSK1 and QPSK2 signals.

IV. Conclusion

In this paper, an all-optical pump-free and reconfigurable M-FC scheme for the input 8QAM signal based on the nonlinear MZI configuration has been proposed and theory simulated for the first time. The input 8QAM signal is divided into two branch signals by the first 3-dB OC. The input lower branch 8QAM signal is rotated by an extra SPM phase shift to obtain the pre-perturbed 8QAM signal. The input upper branch 8QAM signal and the pre-perturbed 8QAM signal can be converted to QPSK1 and QPSK2 by the designed nonlinear MZI configurations, respectively. Various kinds of the aggregated optical signals can be received through the last 3-dB OC after coherent addition between QPSK1 and QPSK2. With the increase of the receiver OSNR, the several aggregated optical signals have worse BER performance than the input 8QAM signal. The two converted QPSK signals have about 3.5 dB and 2.6 dB improvement in receiver OSNR separately comparing with the 8QAM signal with an input OSNR of 25 dB. Compared to the ideal input 8QAM signal with BTB transmission, the two converted QPSK signals have 0.8 dB and 1.7 dB penalty in the receiver OSNR, respectively. This scheme can also be extended to the MFC of the input MQAM signal with two-ring amplitude level, e. g., star-16QAM signals.

The proposed MFC scheme without any extra pump light can be applied at the interface connecting the different types of optical networks, e. g., the gateway between wide area networks (WANs) and local access networks (LANs). Simultaneously, the scheme may be helpful to the all-optical signal regeneration of the advanced modulated signal, e. g., 8QAM signals and 16QAM signals, through regenerating the converted simple optical modulated signals assisted by the PSA technology. The format conversion from the input 8QAM signal to the polarization division multiplexing-QPSK (PDM-QPSK) signal can also be performed by adjusting the polarization state orthogonal of QPSK1 and QPSK2 and coupling them together by one polarization beam combiner (PBC). More noteworthily, the proposed format scheme has a potential advantage in processing multiple wavelength division multiplexing (WDM) channels simultaneously.

Acknowledgment

We acknowledge the reviewers and editors for their careful and constructive suggestions. Qiankun Li would like to thank his parents and friend Hao Zhang for happiness, company and support in the year 2020.

References

[1] W. Lautenschlaeger, N. Benzaoui, F. Buchali, L. Dembeck, R. Dischler, B. Franz, U. Gebhard, J. Milbrandt, Y. Pointurier, D. Roesener, L. Schmalen, and A. Leven, "Optical Ethernet—Flexible Optical Metro Networks," *J. Lightwave Technol.*, vol. 35, no. 12, pp. 2346–2357, Jun 2017.

[2] X. Liu, "Evolution of Fiber-Optic Transmission and Networking toward the 5G Era," *iScience*, vol. 22, pp. 489–506, December 2019.

[3] Q. Li, X. Yang, and J. Yang, "All-Optical Aggregation and De-Aggregation Between 8QAM and BPSK Signal Based on Nonlinear Effects in HNLF," *J. Lightwave Technol.*, vol. 39, no. 17, pp. 5432–5438, Sep 2021.

[4] X. Liu, "Enabling Optical Network Technologies for 5G and Beyond," *J. Lightwave Technol.*, vol. 40, no. 2, pp. 358–367, Jan 2022.

[5] Y. Ji, H. Wang, J. Cui, M. Yu, Z. Yang, and L. Bai, "All-optical signal processing technologies in flexible optical networks," *Photonic Network Communications*, vol. 38, pp. 14–36, 08 2019.

[6] A. E. Willner, A. Fallahpour, K. Zou, F. Alishahi, and H. Zhou, "Optical Signal Processing Aided by Optical Frequency Combs," *IEEE Journal of Selected Topics in Quantum Electronics*, vol. 27, no. 2, pp. 1–16, 2021.

[7] T. Ahmed, S. Rahman, S. Ferdousi, M. Tornatore, A. Mitra, B. C. Chatterjee, and B. Mukherjee, "Dynamic routing, spectrum, and modulation-format allocation in mixed-grid optical networks," *J. Opt. Commun. Netw.*, vol. 12, no. 5, pp. 79–88, May 2020.

[8] X. Zhou and J. Yu, "Multi-Level, Multi-Dimensional Coding for High-Speed and High-Spectral-Efficiency Optical Transmission," *J. Lightwave Technol.*, vol. 27, no. 16, pp. 3641–3653, Aug 2009.

[9] Q. Li and P. Lin, "Re-configurable Optical aggregator of Generating 8QAM and 8PSK Signal," in *Asia Communications and Photonics Conference (ACPC) 2019*. Optica Publishing Group, 2019, p. M4A.62.

[10] M. Klinkowski and K. Walkowiak, "On Performance Gains of Flexible Regeneration and Modulation Conversion in Translucent Elastic Optical Networks With Superchannel Transmission," *J. Lightwave Technol.*, vol. 34, no. 23, pp. 5485–5495, Dec 2016.

[11] H. Guo, Y. Li, L. Li, and G. Shen, "Adaptive Modulation and Regeneration-Aware Routing and Spectrum Assignment in SBPP-Based Elastic Optical Networks," *IEEE Photonics Journal*, vol. 9, no. 2, pp. 1–15, 2017.

[12] D. Hai, T.-M. Hoang, and L. Chau, "QoS-aware protection in elastic optical networks with distance-adaptive and reconfigurable modulation formats," *Optical Fiber Technology*, vol. 61, p. 102364, Nov 2020.

[13] Ken, MISHINA, Daisuke, HISANO, Akihiro, and MARUTA, "All-Optical Modulation Format Conversion and Applications in Future Photonic Networks," *IEICE Transactions on Electronics*, vol. E102.C, no. 4, pp. 304–315, Sep 2019.

[14] F. D. Ros, K. Dalgaard, L. Lei, J. Xu, and C. Peucheret, "QPSK-to-2×BPSK wavelength and modulation format conversion through phase-sensitive four-wave mixing in a highly nonlinear optical fiber," *Opt. Express*, vol. 21, no. 23, pp. 28 743–28 750, Nov 2013.

[15] L. Pan, H. Wang, and Y. Ji, "All-optical deaggregation from 8PSK to 3×BPSK based on FWM in HNLF," *Appl. Opt.*, vol. 58, no. 5, pp. 1246–1252, Feb 2019.

[16] K. Mishina, S. M. Nissanka, A. Maruta, S. Mitani, K. Ishida, K. Shimizu, T. Hatta, and K. ichi Kitayama, "All-optical modulation format conversion from NRZ-OOK to RZ-QPSK using parallel SOA-MZI OOK/BPSK converters," *Opt. Express*, vol. 15, no. 12, pp. 7774–7785, Jun 2007.

[17] G. Huang, Y. Miyoshi, A. Maruta, Y. Yoshida, and K.-I. Kitayama, "All-Optical OOK to 16-QAM Modulation Format Conversion Employing Nonlinear Optical Loop Mirror," *J. Lightwave Technol.*, vol. 30, no. 9, pp. 1342–1350, May 2012.

[18] A. Fallahpour, F. Alishahi, K. Zou, Y. Cao, A. Almaiman, A. Kordts, M. Karpov, M. H. P. Pfeiffer, K. Manukyan, H. Zhou, P. Liao, C. Liu, M. Tur, T. J. Kippenberg, and A. E. Willner, "Demonstration of Tunable Optical Aggregation of QPSK to 16-QAM Over Optically Generated Nyquist Pulse Trains Using Nonlinear Wave Mixing and a Kerr Frequency Comb," *J. Lightwave Technol.*, vol. 38, no. 2, pp. 359–365, Jan 2020.

[19] A. Fallahpour, A. Mohajerin-Ariaei, A. Almaiman, Y. Cao, F. Alishahi, C. Bao, P. Liao, M. Ziyadi, B. Shamee, D. Starodubov, M. Tur, C. Langrock, M. M. Fejer, J. Touch, and A. E. Willner, "Demonstration of 30Gbit/s QPSK-to-PAM4 Data-Format and Wavelength Conversion to Enable All-Optical Gateway from Long-haul to Datacenter," in *Optical Fiber Communication Conference*. Optica Publishing Group, 2018, p. W2A.22.

[20] T. Kodama and T. Miyazaki, "Scalable PAM8 to 8PSK Optical Modulation Format Conversion based on XPM in HNLF at Gateway for Short-reach and Long-haul Integrated NWs," in *Asia Communications and Photonics Conference (ACPC) 2019*. Optica Publishing Group, 2019, p. S3A.5.

[21] Q. Li, J. Yang, X. Yang, Q. Xu, H. Zhang, Y. Liang, and H. Yang, "All-Optical Format Conversion of 2-Dimensional MQAM to MPSK Based on Nonlinear Mach-Zehnder Interferometer With Wavelength Preservation," *J. Lightwave Technol.*, vol. 40, no. 22, pp. 7246–7253, Nov 2022.

[22] Q. Li, X. Yang, H. Wen, Q. Xu, J. Yang, and H. Yang, "All-Optical Format Conversion for Star-8QAM Signals Based on Nonlinear Effects in Elastic Optical Networks," *Journal of Lightwave Technology*, vol. 41, no. 2, pp. 440–450, Jan 2023.

[23] C. Yan, T. Ye, and Y. Su, "All-optical regenerative NRZ-OOK-to-RZ-BPSK format conversion using silicon waveguides," *Opt. Lett.*, vol. 34, no. 1, pp. 58–60, Jan 2009.

[24] A. G. Striegler and B. Schmauss, "Analysis and Optimization of SPM-Based 2R Signal Regeneration at 40 Gb/s," *J. Lightwave Technol.*, vol. 24, no. 7, p. 2835, Jul 2006.

[25] K. Sponsel, C. Stephan, G. Onishchukov, B. Schmauss, and G. Leuchs, "Compensation of Nonlinear Phase Noise Using the Effective Negative Nonlinearity of a Nonlinear Amplifying Loop Mirror," *IEEE Journal of Selected Topics in Quantum Electronics*, vol. 18, no. 2, pp. 637–645, 2012.

[26] Q. Li and P. Zhu, "All-Optical De-aggregation of 4-Level APSK to 2×BPSK Signals Based on SPM and XPM using HNLF," in *Asia Communications and Photonics Conference (ACPC) 2019*. Optica Publishing Group, 2019, p. M4A.57.

[27] B. Lavigne, M. Lefrançois, O. Bertran-Pardo, M. L. Monnier, L. Raddatz, S. Weisser, R. Peruta, G. A. Azzini, and L. Suberini, "Real-time 200 Gb/s 8-QAM transmission over a 1800-km long SSMF-based system using add/drop 50 GHz-wide filters," in *Optical Fiber Communication Conference*. Optica Publishing Group, 2016, p. W3G.2.

[28] J. Zhang, J. Yu, and H.-C. Chien, "Linear and Nonlinear Compensation for 8-QAM SC-400G Long-Haul Transmission Systems," *J. Lightwave Technol.*, vol. 36, no. 2, pp. 495–500, Jan 2018.

[29] M. Nölle, F. Frey, R. Elschner, C. Schmidt-Langhorst, A. Napoli, and C. Schubert, "Performance Comparison of Different 8QAM Constellations for the Use in Flexible Optical Networks," in *Optical Fiber Communication Conference*. Optica Publishing Group, 2014, p. W3B.2.

[30] P. Song, Z. Hu, and C.-K. Chan, "Performance Comparison of Different 8-QAM Constellations Used in SEFDM systems," in *2021 Opto-Electronics and Communications Conference (OECC)*, Jul 2021, pp. 1–3.

[31] L. Nadal, J. M. Fbrega, J. Vłlchez, and M. Svaluto Moreolo, "Experimental Analysis of 8-QAM Constellations for Adaptive Optical OFDM Systems," *IEEE Photonics Technology Letters*, vol. 28, no. 4, pp. 445–448, 2016.

[32] J. Zhao, C. Qin, M. Zhang, and N. Chi, "Investigation on performance of special-shaped 8-quadrature amplitude modulation constellations applied in visible light communication," *Photon. Res.*, vol. 4, no. 6, pp. 249–256, Dec 2016.

[33] Y. Wan, B. Liu, J. Ren, R. Ullah, Y. Mao, S. Zhu, S. Chen, X. Wu, F. Wang, T. Sun, Y. Wu, and L. Zhao, "Performance-Enhanced Optical Non-Orthogonal Multiple Access Enabled by Orthogonal Chirp Division Multiplexing," *J. Lightwave Technol.*, vol. 40, no. 16, pp. 5440–5449, Aug 2022.

[34] H. X. Z. J. N. W. L. Q. C. N. LI Zhongya, CHEN Rui, "SVM for Constellation Shaped 8QAM PON System," *ZTE Communication: English*, vol. 020, pp. 64–71, Sep 2022.

[35] X. Pan, Y. Liu, and L. Guo, "Asymmetric constellation transmission for a coherent free-space optical system with spatial diversity," *Opt. Lett.*, vol. 46, no. 20, pp. 5157–5160, Oct 2021.

[36] B. Zhang, H. Zhang, C. Yu, X. Cheng, Y. K. Yeo, P.-K. Kam, J. Yang, H. Zhang, Y.-H. Wen, and K.-M. Feng, "An All-Optical Modulation Format Conversion for 8QAM Based on FWM in HNLF," *IEEE Photonics Technology Letters*, vol. 25, no. 4, pp. 327–330, 2013.

[37] H. Liu, H. Wang, and Y. Ji, "Simultaneous All-Optical Channel Aggregation and De-Aggregation for 8QAM Signal in Elastic Optical Networking," *IEEE Photonics Journal*, vol. 11, no. 1, pp. 1–8, Feb 2019.

[38] H. Kishikawa, M. Uetai, and N. Goto, "All-Optical Modulation Format Conversion Between OOK, QPSK, and 8QAM," *J. Lightwave Technol.*, vol. 37, no. 16, pp. 3925–3931, Aug 2019.

[39] Z. Zhong, H. Wang, and Y. Ji, "All-optical aggregation and de-aggregation between 3 × BPSK and 8QAM in HNLF with wavelength preserved," *Appl. Opt.*, vol. 59, no. 4, pp. 1092–1098, Feb 2020.

[40] B. Stiller, G. Onishchukov, B. Schmauss, and G. Leuchs, "Phase regeneration of a star-8QAM signal in a phase-sensitive amplifier with conjugated pumps," *Opt. Express*, vol. 22, no. 1, pp. 1028–1035, Jan 2014.

[41] H. Liu, H. Wang, Z. Xing, and Y. Ji, "Simultaneous all-optical channel aggregation and de-aggregation based on nonlinear effects for OOK and MPSK formats in elastic optical networking," *Opt. Express*, vol. 27, no. 21, pp. 30 158–30 171, Oct 2019.

[42] H. Wang, G. Li, and Y. Ji, "Phase and amplitude regeneration of a rectangular 8-QAM in a phase-sensitive amplifier with low-order harmonics," *Appl. Opt.*, vol. 56, no. 3, pp. 506–509, Jan 2017.

[43] Q. Li, H. Zhang, Z. Liu, and S. Fu, "SPM-based Data Format Conversion from one 2ASK/4PSK to two 4PSK Signals with Wavelength Preservation," in *Asia Communications and Photonics Conference 2021*. Optica Publishing Group, 2021, p. T4A.87.

[44] V. Krishnamurthy, Y. Chen, and Q. Wang, "MZI-Semiconductor-Based All-Optical Switch With Switching Gain," *J. Lightwave Technol.*, vol. 32, no. 13, pp. 2433–2439, Jul 2014.

[45] X. Kong, B. Wu, X. Zhou, Q. Wan, S. Jiang, F. Wen, and K. Qiu, "Design of all-optical multi-level regenerators based on Mach-Zehnder interferometer," *Optics Communications*, vol. 380, pp. 377–381, Dec 2016.

[46] S. Wabnitz and B. J. Eggleton, "[Springer Series in Optical Sciences] All-Optical Signal Processing Volume 194 —— Optical Guided Wave Switching," no. Chapter 3, pp. 71–104, 2015.

[47] G. B. Xavier and J. P. von der Weid, “Stable single-photon interference in a 1 km fiber-optic Mach–Zehnder interferometer with continuous phase adjustment,” *Opt. Lett.*, vol. 36, no. 10, pp. 1764–1766, May 2011.

[48] S.-B. Cho and T.-G. Noh, “Stabilization of a long-armed fiber-optic single-photon interferometer,” *Opt. Express*, vol. 17, no. 21, pp. 19 027–19 032, Oct 2009.

[49] N. J. Doran and D. Wood, “Nonlinear-optical loop mirror,” *Opt. Lett.*, vol. 13, no. 1, pp. 56–58, Jan 1988.

[50] F. Parmigiani, L. Jones, J. Kakande, P. Petropoulos, and D. J. Richardson, “Modulation format conversion employing coherent optical superposition,” *Opt. Express*, vol. 20, no. 26, pp. B322–B330, Dec 2012.